Preprints.org

Article

Not peer-reviewed version

From Isotopic Evidence to Economic Valuation: A 'Water-Carbon-Economy' Nexus Framework for Climate-Resilient Urban Forestry, Southwestern China

Jiaojiao Han *, Yan Zhong , Ziying Sun , Xuejie Wang , Yingzhu Yang

Posted Date: 28 January 2026

doi: 10.20944/preprints202601.2161.v1

Keywords: urban forestry; stable isotopes; water use efficiency; ecosystem service valuation; urban water economics; climate-resilient greening

Preprints.org is a free multidisciplinary platform providing preprint service that is dedicated to making early versions of research outputs permanently available and citable. Preprints posted at Preprints.org appear in Web of Science, Crossref, Google Scholar, Scilit, Europe PMC.

Copyright: This open access article is published under a Creative Commons CC BY 4.0 license, which permit the free download, distribution, and reuse, provided that the author and preprint are cited in any reuse.

Preprints.org (www.preprints.org) | NOT PEER-REVIEWED | Posted: 28 January 2026 doi:10.20944/preprints202601.2161.v1

Disclaimer/Publisher's Note: The statements, opinions, and data contained in all publications are solely those of the individual author(s) and contributor(s) and not of MDPI and/or the editor(s). MDPI and/or the editor(s) disclaim responsibility for any injury to people or property resulting from any ideas, methods, instructions, or products referred to in the content.

Article

From Isotopic Evidence to Economic Valuation: A 'Water-Carbon-Economy' Nexus Framework for Climate-Resilient Urban Forestry, Southwestern China

Jiaojiao Han [1,*], Yan Zhong [1], Ziying Sun [1], Xuejie Wang [2] and Yingzhu Yang [3]

[1] College of Economics and Management, Baoji University of Arts and Sciences, Baoji, Shanxi 721013, China

[2] College of Agriculture Forestry Ecology, Shaoyang University, Shaoyang, Hunan 422000, China

[3] College of Marxism, Yunnan University, Kunming, Yunnan 650500, China

* Correspondence: hanjiaojiao@bjwlxy.edu.cn

Abstract

Optimizing public investment in urban green infrastructure under water scarcity is a core challenge in resource economics. This study addresses the critical knowledge gap in quantifying the economic returns on physiological adaptations of urban trees, which are central to their value as natural capital. We integrate dual water isotopes (δ^2H, $\delta^{18}O$) and leaf carbon isotope ($\delta^{13}C$) analysis to mechanistically decode the water-use strategy of *Machilus yunnanensis* in drought-prone Kunming, China. Results show strategic seasonal plasticity: a shift from shallow soil water (10–50 cm) in the wet season to deeper soil sources (50–90 cm) and stem reserves in the dry season, coupled with a dynamic, diurnally variable water-use efficiency (WUE). We then construct a transparent economic valuation model translating these traits into three quantifiable benefit streams: (1) Operational cost savings (EV_1) from reduced irrigation demand; (2) Enhanced marginal productivity of water (EV_2) in ecosystem service generation; and (3) Climate resilience value (EV_3) via mitigated mortality risk. Our "Water-Carbon-Economy" nexus framework provides a generalizable methodology for assessing the cost-effectiveness and risk-adjusted returns of urban forest species. It demonstrates that selecting trees based on such eco-efficient traits is not merely an ecological choice but a sound economic investment, offering direct implications for budget-constrained municipalities seeking to maximize the benefits of green infrastructure under climate uncertainty.

Keywords: urban forestry; stable isotopes; water use efficiency; ecosystem service valuation; urban water economics; climate-resilient greening

1. Introduction

Against the backdrop of global climate change and rapid urbanization, the management of urban green spaces has evolved from an aesthetic concern to a critical socio-economic investment in public health, climate resilience, and sustainable resource use (United Nations Environment Programme, 2021). With over 80 major cities experiencing extreme drought in recent decades and urban populations projected to reach 70% of the global total by 2050, the economic pressure on municipal water budgets is intensifying. Urban trees, while providing invaluable ecosystem services such as carbon sequestration, air purification, and urban heat island mitigation, also represent a significant water demand (Nowak, 2023; Egerer et al., 2024). Therefore, optimizing the water-use efficiency (WUE) of urban greenery is not merely an ecological question but a core issue of resource economics and natural capital management, directly impacting the cost-effectiveness, risk profile, and long-term viability of green infrastructure investments (Qi et al., 2025). This framing positions urban forestry as a portfolio of biological assets, where selecting species with high resource-use

© 2025 by the author(s). Distributed under a Creative Commons CC BY license.

Preprints.org (www.preprints.org) | NOT PEER-REVIEWED | Posted: 28 January 2026 doi:10.20944/preprints202601.2161.v1

efficiency is akin to choosing investments with superior risk-adjusted returns (Fenichel & Abbott, 2014).

Empirical evidence underscores this urgency, confirming that urban trees experience greater growth decline than rural trees due to amplified water stress (Wu et al., 2025). Yet, the species-specific physiological strategies—such as dynamic water source partitioning and efficiency adjustments—that underpin such vulnerability or resilience remain poorly quantified. This knowledge gap represents a critical economic analytical shortfall: it fundamentally limits the development of evidence-based management protocols and, more specifically, hinders the quantification of the economic returns on physiological adaptation—a key parameter for optimizing public investment in climate-resilient natural capital.

Stable isotope techniques, particularly using dual isotopes of hydrogen and oxygen (δ^2H and $\delta^{18}O$), have become powerful tools for tracing water movement within the Soil-Plant-Atmosphere Continuum (SPAC), identifying plant water uptake depths, and quantifying the contribution of different sources (Gao et al., 2024; Zhang et al., 2022; Han et al., 2022). Concurrently, leaf carbon isotope composition ($\delta^{13}C$) serves as a reliable proxy for long-term intrinsic Water Use Efficiency (WUE). Integrating dual water isotopes with carbon isotope analysis allows a systematic investigation of plant survival strategies from the two dimensions of water acquisition ("source") and utilization efficiency ("sink"). This precise quantification forms the scientific basis for informed water resource management and cost-benefit analysis (Li et al., 2024; Durodola et al., 2025). When viewed through an economic lens, these isotopic metrics provide the essential biophysical micro-foundations for modeling input substitution, marginal productivity of water, and adaptive capacity. Research applications have advanced in natural ecosystems, and economic analyses have demonstrated the cost-effectiveness of alternative irrigation sources like reclaimed water (Liu et al., 2025; Lv et al., 2021; Santos et al., 2025).

However, critical gaps persist at the intersection of precise ecohydrological mechanism elucidation and practical socio-economic valuation, especially for urban greening. First, targeted research on dominant urban greening tree species in specific climatic regions—particularly in monsoon-influenced areas with pronounced seasonal drought—remains scarce. Second, and most pertinent to resource economics, a fundamental disconnect remains: existing ecohydrological studies often lack formal economic integration, failing to translate physiological adaptations into standardized economic metrics such as marginal irrigation cost savings, the enhanced marginal value product of water in service delivery, or the option value of reduced mortality risk (Shi et al., 2021; Salmani et al., 2025). Conversely, socio-economic assessments frequently lack the granular, species-specific physiological data needed to justify and optimize management investments (Kudaya et al., 2025). For example, while the socio-economic value of green spaces for mitigating waterlogging is recognized (Yang et al., 2025), the fundamental question of how a specific tree species' inherent water-use strategy directly influences its cost-effectiveness and resilience dividend remains an unresolved empirical and theoretical question in environmental investment analysis.

To address this critical gap, this study takes *Machilus yunnanensis*—a keystone native evergreen broadleaf tree widely planted in drought-prone Kunming, southwestern China—as a model system. Kunming, characterized by a subtropical plateau monsoon climate, experiences over 80% of its annual precipitation during the wet season (May–October), leaving a prolonged dry season (Zhu et al., 2021). While empirically considered adaptable, a systematic, mechanistic understanding of its water-use strategy is lacking, hindering both evidence-based planning and a clear economic valuation of its adaptation traits. We conducted comprehensive year-round field monitoring from July 2020 to July 2021, employing a dual-isotope (δ^2H and $\delta^{18}O$) approach to analyze various water pools alongside leaf $\delta^{13}C$ to monitor intrinsic WUE. The objectives are threefold: (1) to quantify seasonal shifts in water source contributions using δ^2H and $\delta^{18}O$; (2) to reveal the diurnal and seasonal dynamics of intrinsic WUE using $\delta^{13}C$; and (3) to explicitly link these physiological strategies to a transparent economic valuation model, thereby bridging the biophysical and economic analysis of urban natural capital. By extending the traditional "Water-Carbon" nexus to a "Water-Carbon-

© 2025 by the author(s). Distributed under a Creative Commons CC BY license.

Preprints.org (www.preprints.org) | NOT PEER-REVIEWED | Posted: 28 January 2026 doi:10.20944/preprints202601.2161.v1

Economy" nexus, this study provides both species-specific evidence and a generalizable framework for assessing the economic efficiency of climate-adaptive traits in urban forestry, contributing directly to the literature on resource management and environmental investment under uncertainty.

2. Materials and Methods

2.1. Site Description

We made observation of water isotopes in precipitation, plant and soil water in July 2020 to July 2021 at the urban forestland located at the campus of Chenggong Campus of Yunnan University (24°49′N, 102°51′E; 1990m above sea level) in Kunming, the middle of Yunnan-Guizhou Plateau, Southwest China (Fig. 1). This region is featured with an altitude monsoon climate, with Indian monsoon intrusion in summer and continental monsoon in winter. The average annual precipitation is 790 mm, with distinctive seasonality of over 85 % of the annual precipitation in summer from June to September, while little precipitation in the dry winter season from November to next April (Zhu et al., 2021). The monthly air temperature varies from 7.7 ℃ in January to 20.6 ℃ in July, with annual average of 14.7 °C (Bi et al., 2018). The primary soil type is red soil (Wang et al., 2016). The forest consists primarily of urban forest, including *M. yunnanensis*, *Pinus yunnanensis*, and *Photinia serrulata*, in addition to some minor components of other woodland species and shrubs, such as *Bougainvillea spectabilis*, *Festuca rubra*, and *Oxalis corniculata*. In this paper, we selected *M. yunnanensis* as the target tree for water sources and water use efficiency observation by using water isotope. The height of the community varies from 3 m to 6 m in the sampling plot. In this study, the growing season is defined as the period from May to September.

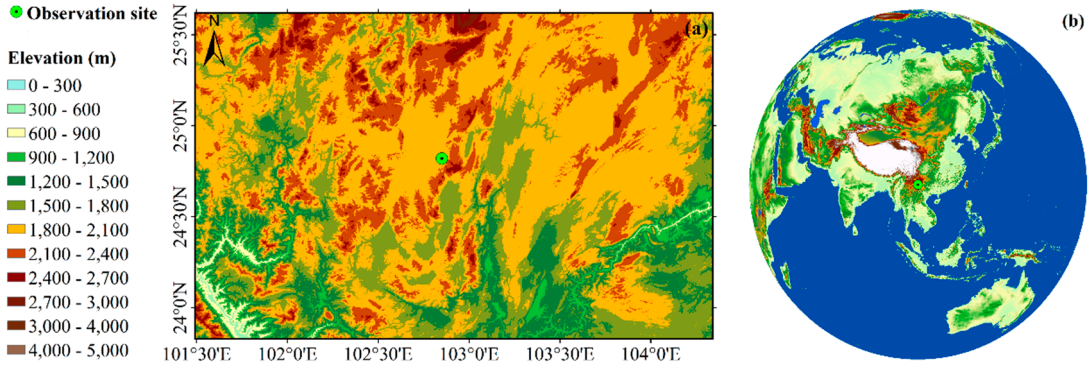

Figure 1. The geographic sitting of the Kunming (a) and its location (marked by a green circle) in the Yunnan-Guizhou Plateau.

2.2. Sampling and Measurement

We performed monitoring of water isotopes in soil water, xylem water, stem water, leaf water simultaneously during July 2020 to July 2021. In each measurement, a hollow-stem auger (Haglöf, Västernorrland, Sweden) was used to collected at 13:00 with a sampling frequency of 1-2 times per month xylem samples of three individuals of *M. yunnanensis* with three replications. All xylem samples were taken at chest-height (Dawson and Ehleringer, 1993). The collected stem samples from the base of the plant (green tissue, e.g., outer leaf) were stripped and only the white (i.e., non-transpiring) tissue was used for measurement, and all stem samples individuals had leaves samples, i.e., they were transpiring water. We measured stem and leaf samples at 9:00, 11:00, 13:00, 15:00, 17:00 and 19:00 at different sides of the tree (east, west, south, north) and from three mature trees for the representative of the measurement. Leaf samples were separated into two parts for hydrogen and oxygen and carbon stable isotope analysis, respectively. The leaf sample collection followed the national standards of “Observation Methodology for Long-term Forest Ecosystem Research from (GB/T33027-2016)”. Soil samples were collected at 13:00 at depth of 5 cm, 10 cm, 20 cm, 30 cm, 40 cm,

© 2025 by the author(s). Distributed under a Creative Commons CC BY license.

Preprints.org (www.preprints.org) | NOT PEER-REVIEWED | Posted: 28 January 2026 doi:10.20944/preprints202601.2161.v1

50cm, 60cm, 70cm, 80cm and 90 cm with three replications at each measurement, with a hand auger at sites near the three trees and the average value was used for representative. All plant (*M. yunnanensis*) and soil samples were measured by the isotope analyzer in solid mode combined with an induction module (IM). The solid mode allowed for the simultaneous measurement of the isotopic compositions of small solid samples and the removal of organic contamination from within the samples in the field (Quade et al., 2019). A measurement of the plant and soil water immediately after sampling will also reduce the influence of evaporation on water isotopes. Three laboratory standard waters were used for calibration: S_1 ($\delta^{18}O$= -2.83 ‰, δ^2H= -27.42 ‰), S_2 ($\delta^{18}O$= -29.84 ‰, δ^2H= -222.84 ‰) and S_3 ($\delta^{18}O$= -15.29 ‰, δ^2H= -110.30 ‰), which roughly cover the ranges of the measured water isotope ratios. The samples were corrected for drift and memory using the procedure described in Geldern and Barth (2012). The measured precision is ± 0.20 ‰ for $\delta^{18}O$ and ± 0.69 ‰ for δ^2H. The detailed measurement and calibration processes followed the protocol of Cui et al. (2017).

We also collected precipitation for isotope measurement as well during the same period nearby on the Yunnan University of campus. Daily precipitation samples were collected at 20:00 in the raining day using a container (Gröning et al., 2012), specifically designed to avoid re-evaporation of collected water samples. All samples were stored in plastic bottles and frozen in refrigerator before laboratory analysis. The collected precipitation samples were analyzed in laboratory by using Picarro L2140-i liquid water isotope analyzer for both $\delta^{18}O$ and δ^2H. All measured results were normalized to VSMOW (Vienna Standard Mean Ocean Water), with precision within ± 0.05 ‰ for $\delta^{18}O$ and ± 0.5 ‰ for δ^2H.

2.3. Micrometeorological Measurements

We installed the eddy covariance (EC) instruments meteorology station in the sampling station, including an open path infrared CO_2/H^2O gas analyzer (Li-7500 A, Li-Cor, USA) and a three-dimensional sonic anemometer thermometer (CSAT3B, Campbell Scientific Inc., USA) mounted 3 m above the ground. The data were stored in a CR6 data logger and CF storage card at a sampling frequency of 10 Hz. The Raw data acquired at 10 Hz were processed using the postprocessing software EdiRe, and quality control of the half-hourly flux data were conducted as described in earlier literature (Xu et al., 2013). Micrometeorological parameters (air temperature, relative humidity, wind speed, precipitation amount, four-component radiation, three layers of soil temperature and soil moisture profiles, soil heat flux, etc.) were recorded under 1 Hz. Additional details concerning data acquisition were described (Liu and Zhang. 2012). Based on measurements from the EC system, the energy balance closure ratio was evaluated at this site, and result shows a relatively high energy balance closure ratio of 0.88, indicating that the energy balance closure problem (Wilson et al., 2001) is not a major concern for the site and system.

2.4. Data Analysis

2.4.1. Contributions of Water from Different Sources to M. yunnanensis.

The MixSIAR model is a stable isotope mixing model to calculate the contribution of different water sources to *M. yunnanensis*. In this study, the direct contrast method and MixSIAR model were used to analyze plant water sources comprehensively. The soil moisture that may be mainly used by plants is directly judged by the method of direct comparison, and the source of plant water is qualitatively analyzed. MixSIAR model was used to estimate the water use ratio of plants to various water sources and the average depth of soil water use, and to quantitatively analyze the sources of plant water. In this study, the water sources were defined as the soil waters in layers from 5cm to 90cm and stem water, and were divided into six groups according to their isotopic composition to represent the potential water sources. Within the MixSIAR program, the increments were set at 2 % solution and a tolerance level of ± 0.05 % was counted as feasible solutions. The sensitivity was analyzed with different fractional increments (0.5, 2 %) and at different uncertainty levels (0.1, 0.3,

© 2025 by the author(s). Distributed under a Creative Commons CC BY license.

Preprints.org (www.preprints.org) | NOT PEER-REVIEWED | Posted: 28 January 2026 doi:10.20944/preprints202601.2161.v1

and 0.4). The results showed no significant differences in changes in fractional increment and uncertainty level.

2.4.2. $\Delta^{13}C$ (Carbon Isotope Discrimination) and Calculation of WUE

The leaf samples were ultrasonically washed with distilled water, air-dried, oven-dried at 60°C for at least 72 h to a constant weight, then ground and finally sieved through a 1-mm mesh screen. We used a Picarro G2201-i (Picarro Inc., Santa Clara, CA) high frequency wavelength-scanned cavity ring-down spectroscopy (WS-CRDS) analyzer for carbon isotope measurement. According to the PDB (belemnite from the Pee Dee Formation) standard. The precision was precision of < 0.12 %. The leaf $\delta^{13}C$ value was determined using the following equation:

$$\delta^{13}C = \left(\frac{R_{sample}}{R_{standard}} - 1\right) \times 1000 \quad (1)$$

where R_{sample} and $R_{standard}$ are the $^{13}C/^{12}C$ ratios in the samples and the PDB (Pee Dee Formation) standard, respectively. (Farquhar et al., 1989).

Isotopic effects can also be expressed by isotopic discrimination values (Δ). Because CO_2 is the source of plant photosynthesis, its photosynthetic discrimination value can be described as follows (Martínez-Sancho et al., 2017):

$$\Delta^{13}C = (\delta^{13}C_a - \delta^{13}C_p)/(1 + \delta^{13}C_p/1000) \quad (2)$$

where $\delta^{13}C_a$ and $\delta^{13}C_p$ represent the $\delta^{13}C$ values of air and plant samples, respectively. The $\delta^{13}C_a$ was assumed to be −8 ‰, according to (Farquhar et al., 1989). In C3 plants, $\Delta^{13}C$ is primarily determined by the ratio of intercellular to ambient leaf CO_2 via the following formula:

$$\Delta^{13}C = a + (b - a)\frac{C_i}{C_a} \quad (3)$$

where a (4.4 ‰) represents the diffusive discrimination of ^{13}C in air through stomata, b (27‰) represents the net discrimination associated with carboxylation, and C_a and C_i are the air and intercellular partial pressures of CO_2, respectively (Farquhar et al., 1989; Maxwell et al., 2018).

In plants, leaf conductance to water vapor (g_{H2O}) is related to the leaf conductance of CO_2 (g_{CO2}) as per the following equation:

$$g_{H2O} = 1.6g_{co2} \quad (4)$$

where 1.6 is the ratio of water vapor to CO_2 diffusivity.

Further, Leaf net photosynthesis (A) is related to g_{H2O} as the following equation:

$$A = g_{co2}(C_a - C_i) \quad (5)$$

where A is net photosynthesis, and g_{CO2} is leaf conductance of CO_2 (Pe˜nuelas et al., 2011).

Given equations (3)-(5), $\Delta^{13}C$ can be converted to the ratio A/g_{H2O} (WUE) via the following equation (Yan et al., 2016):

$$WUE = \frac{A}{g_{H2O}} = \frac{b - \Delta^{13}C}{1.6(b - a)} \quad (6)$$

2.5. Economic Valuation Framework

The economic value (EV) of *M. yunnanensis*'s adaptive strategy is disaggregated into three components, each derived from the isotopic and physiological data. This translation from biophysical traits to economic metrics addresses a core need in environmental accounting: moving from qualitative descriptions of ecosystem services to quantitative, marginal analyses of resource use efficiency (Boyd & Banzhaf, 2007).

EV_1: Operational Cost Savings from Irrigation Substitution. This represents the avoided cost of supplemental watering due to the tree's ability to access deeper soil water and stem reserves during drought, a direct application of the concept of input substitution in production economics.

$$EV_1 = \Delta V_irri \times P_water + \Delta C_maint \quad (7)$$

where ΔV_irri is the volume of irrigation water substituted, estimated from the MixSIAR-modeled shift in water source proportions (Fig. 10) and local evapotranspiration estimates. P_water is the

© 2025 by the author(s). Distributed under a Creative Commons CC BY license.

Preprints.org (www.preprints.org) | NOT PEER-REVIEWED | Posted: 28 January 2026 doi:10.20944/preprints202601.2161.v1

marginal price of municipal irrigation water. ΔC_maint encompasses saved labor and energy costs from reduced irrigation frequency.

EV_2: Value of Enhanced Water Productivity. Higher intrinsic WUE implies greater ecosystem service output per unit of water transpired, reflecting an increase in the total factor productivity of the water input. We focus on carbon sequestration as a representative service.

$EV_2 = (\Delta A / \Delta g_H2O) \times V_C$ (8)

where the ratio ($\Delta A / \Delta g_H2O$) is the change in net carbon assimilation per change in water loss, derived from the $\delta^{13}C$-WUE relationship (Eq. 6). V_C is the social or market value of sequestered carbon (e.g., shadow price from integrated assessment models or local carbon trading schemes).

EV_3: Climate Resilience Value. This captures the avoided loss from reduced drought-induced mortality, modeled as a risk premium analogous to the option value of adaptation in environmental economics.

$EV_3 = (R_mortality \times V_replacement) \times (1 - \theta_adapt)$ (10)

where R_mortality is the baseline annual mortality risk for non-adapted species under drought stress, V_replacement is the net present cost of sapling purchase, planting, and establishment, and θ_adapt ($0 \le \theta \le 1$) is the relative risk reduction factor attributed to the species' adaptive plasticity, inferred from its sustained physiological function during the observed dry period.

Sensitivity & Uncertainty: Key parameters (P_water, V_C, R_mortality) are assigned plausible ranges based on local market data and literature. A Monte Carlo simulation is recommended for full implementation to propagate uncertainty from both isotopic and economic parameters. The primary contribution of this section is the development of a transparent, replicable valuation model that parameterizes economic value directly with biophysical measurements, providing a concrete method for assessing urban trees as productive natural capital assets (Fenichel & Abbott, 2014).

3. Results

3.1. Seasonal Variation of Environmental Variables

Detailed information on the seasonality of the environmental variables is essential to assess seasonal variations in quantifying water sources and water use efficiency. Fig. 2 shows the seasonal variations of daily air temperature (Ta), relative humidity (RH), vapor pressure deficit (VPD), wind speed (u), daily sum of precipitation amount (P) and volumetric soil water content (θ) at different depth from the in-situ flux observation. As Fig. 2(a) shows the seasonal variation of Ta and RH during monitoring period. Daily air temperature was 17.0 in the monitoring period, varying from -1.9 to -24.5°C. RH was 64.9 in the monitoring period, varying from 24.8 to 97.2. The seasonal variation of VPD and u during monitoring period (Fig. 2b). Daily wind speed was 0.6 m s^{-1} in the monitoring period, varying from 0.1 to 1.7 m s^{-1}. Mean vapor pressure deficit varied between 0.1 and 2.2 Kpa. Fig. 2(c) exhibits the seasonal variations of daily average precipitation and soil moisture content. Daily average precipitation was 2.4 mm d^{-1}. Although we only have the observation of soil moisture at shallow surface, it can reflect the root zone moisture as well. Daily averaged θ at the was maintained at a high level during the observation period. The large fluctuation of soil moisture content at a depth of 5 cm is caused by rapid evaporation and precipitation replenishment. While the soil moisture content is quite constant in 40 cm depth, and slight variations is in response to precipitation events but with lag of a couple of days.

© 2025 by the author(s). Distributed under a Creative Commons CC BY license.

Preprints.org (www.preprints.org) | NOT PEER-REVIEWED | Posted: 28 January 2026 doi:10.20944/preprints202601.2161.v1

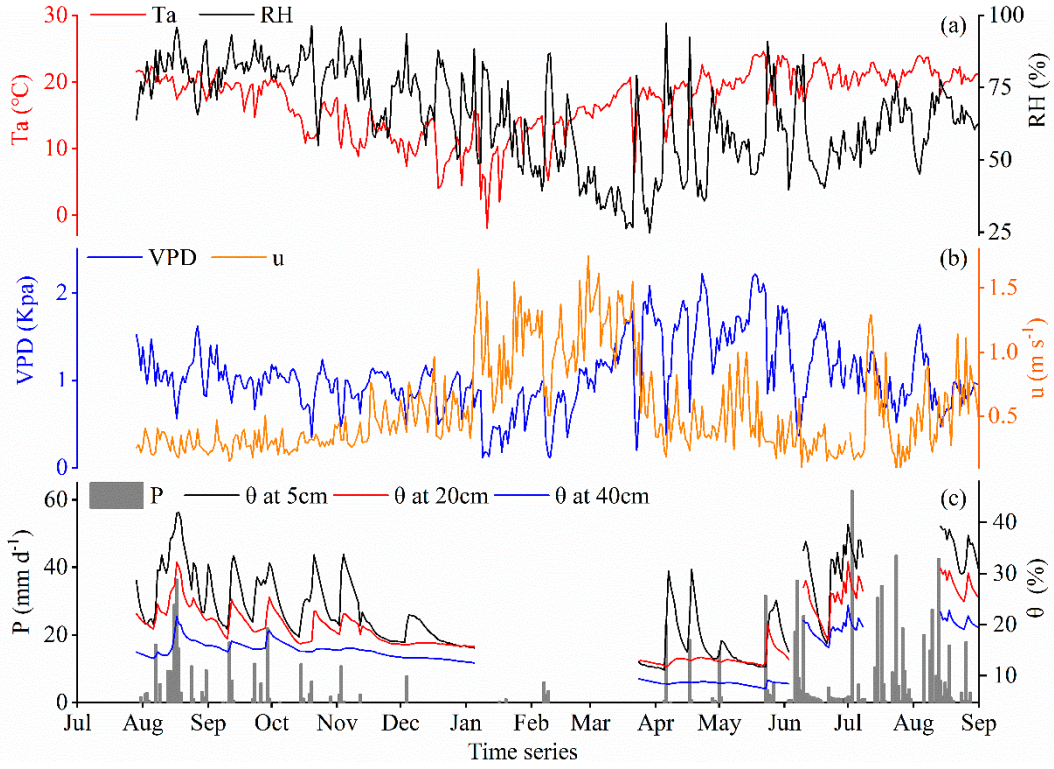

Figure 2. Seasonal variations in (a) daily mean temperature (Ta) and relative humidity (RH); (b) vapor pressure deficit (VPD) and wind speed (u); and (c) daily sum of precipitation amount (P) and volumetric soil water content (θ) at 5 cm depth (blue line), 20 cm depth (red line) and 40 cm depth (black line) during the observations. The volumetric soil water content data were unavailable from 5 January to 24 March 2021, from 4 to 9 June 2021, and from 9 July to 13 August 2021 due to soil moisture monitoring probe failure.

3.2. *Relationship Between $\delta^{18}O$ and $\delta^{2}H$ of Different Water Pools*

The dual-isotope plot ($\delta^{2}H$-$\delta^{18}O$) reveals distinct fractionation patterns across ecosystem water pools, reflecting their respective hydrological processes (Good et al., 2015). The local meteoric water line (LMWL), defined as $\delta^{2}H = 8.22\ \delta^{18}O + 11.52$ ($R^2 = 0.99$, $p < 0.001$, n=145) (Fig. 3), is consistent with the Global Meteoric Water Line (GMWL; Craig, 1961; Rozanski et al., 1993). In contrast, soil water samples ($\delta^{18}O$: -14.10 to -4.72‰; $\delta^{2}H$: -117.91 to -42.24‰) deviate below the LMWL, forming a soil water line (SWL: $\delta^{2}H = 7.52\delta^{18}O - 7.15$; $R^2 = 0.65$, $p < 0.001$, n=109). This lower slope and intercept indicate significant evaporative enrichment post-infiltration, despite some moderation by vegetation cover (Dubbert et al., 2013). Plant water isotopes demonstrate a progressive enrichment sequence. The xylem water line (XWL: $\delta^{2}H = 5.95\delta^{18}O - 26.67$; $R^2 = 0.81$, $p < 0.001$, n=41) plots intermediately between soil and stem water. Further isotopic enrichment is observed in stem water (STWL: $\delta^{2}H = 4.77\delta^{18}O - 40.76$; $R^2 = 0.65$, $p < 0.001$, n=216) and culminates in leaf water (LWL: $\delta^{2}H = 3.21\delta^{18}O - 55.30$; $R^2 = 0.70$, $p < 0.001$, n=216). The successively lower slopes and more negative intercepts from the SWL to the LWL quantitatively trace the strong gradient of evaporative fractionation through the Soil-Plant-Atmosphere Continuum, with leaf water exhibiting the most pronounced isotopic enrichment during transpiration.

© 2025 by the author(s). Distributed under a Creative Commons CC BY license.

Preprints.org (www.preprints.org) | NOT PEER-REVIEWED | Posted: 28 January 2026 doi:10.20944/preprints202601.2161.v1

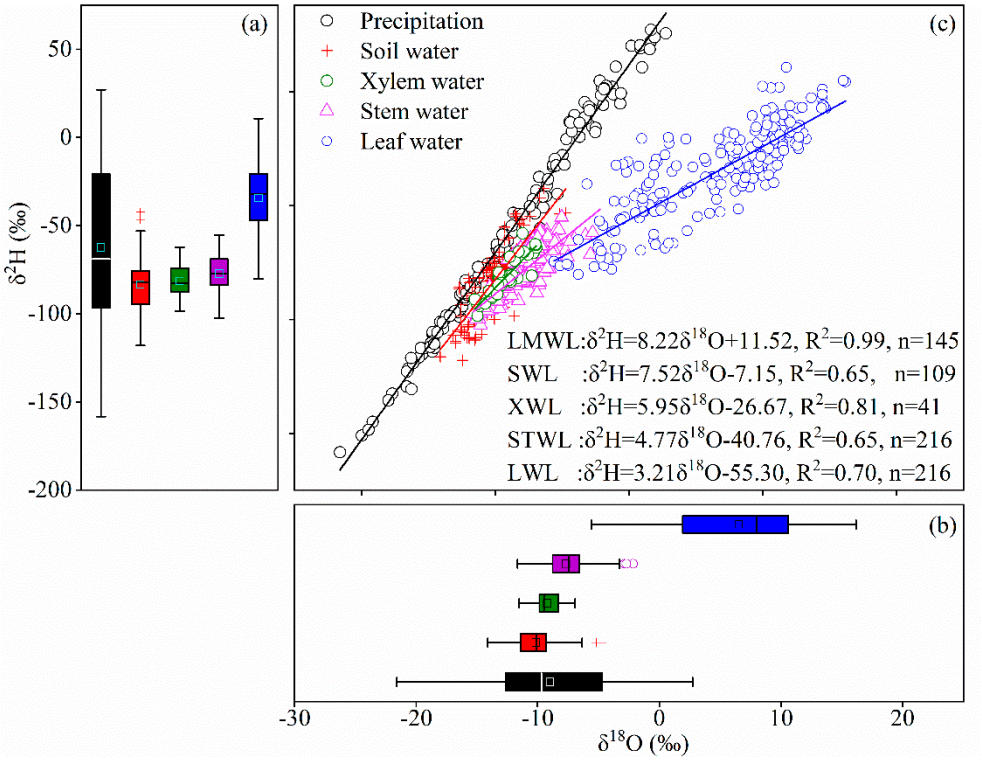

Figure 3. $\delta^{18}O$ versus $\delta^{2}H$ in precipitation (open black circles), soil water (red black circles), xylem water (open green circles), stem water (open purple circles) and leaf water (open blue circles). (a) and (b) are the $\delta^{18}O$ and $\delta^{2}H$ of different water bodies, respectively, and (c) is the linear regression line of $\delta^{18}O$ and $\delta^{2}H$ in different water pools. The box indicates the 25th and 75th percentiles with the median as thick black line and the average as square. The error bars indicate the minimum and maximum values. The circles indicate outliers (3/2 times the central box).

3.3. Seasonal Variation of Precipitation Isotopes in the Forest Ecosystem

Since the seasonal variations of hydrogen and oxygen stable isotopes are mainly consistent, using $\delta^{18}O$ solely to identify the seasonal variations of the stable isotopic composition is reasonable. We presented the daily precipitation $\delta^{18}O$ and d-excess and precipitation amount from Kunming (Fig. 4). The daily isotopic composition of the precipitation samples ranges from −21.6 to 2.7 ‰ for $\delta^{18}O$ (−9.0 ‰ in average) and from -6.9 to 22.4 ‰ for d-excess (9.5 ‰ in average). Precipitation $\delta^{18}O$ shows a seasonal shift from the higher value in the earlier summer of January-June to the lower $\delta^{18}O$ period of the raining season until to October. This seasonal precipitation is consistent with the seasonal feature of monsoon type precipitation signal. The seasonal variation of precipitation d-excess shows an opposite trend to $\delta^{18}O$ changes, likely a signal of enhancing evaporation enrichment of precipitation, precipitation during the dry season in spring and early summer. Slight lower precipitation d-excess in less rainfall days are probably related to the reevaporation of falling raindrops, which lowered d-excess in the left rainfall.

© 2025 by the author(s). Distributed under a Creative Commons CC BY license.

Preprints.org (www.preprints.org) | NOT PEER-REVIEWED | Posted: 28 January 2026 doi:10.20944/preprints202601.2161.v1

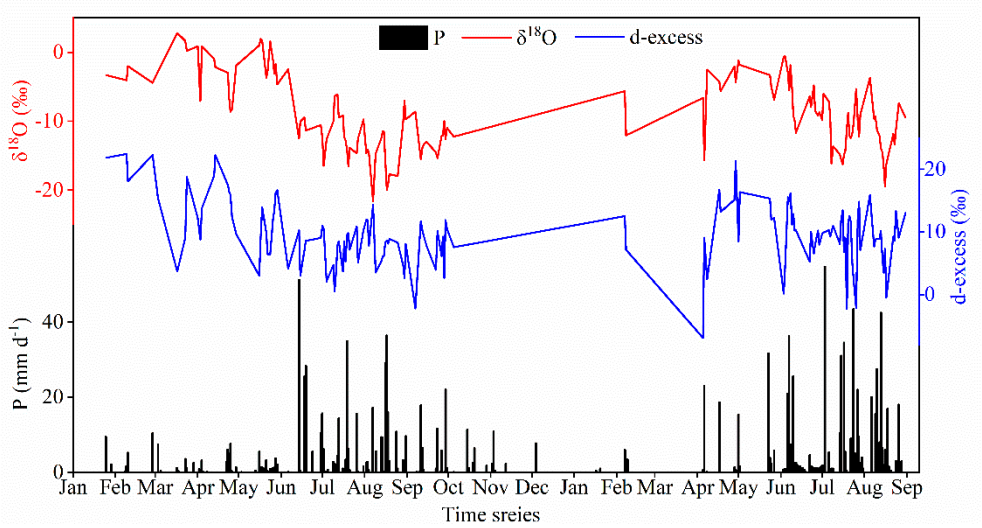

Figure 4. Daily precipitation $\delta^{18}O$ and d-excess as comparison with precipitation amount in Kunming during July 2020-September 2021.

3.4. Isotopic Composition of Soil Water at Different Depths

The isotopic composition of soil water revealed distinct vertical stratification and contrasting seasonal dynamics between shallow and deep layers (Fig. 5). Soil water $\delta^{18}O$ values ranged from −14.1‰ to −4.7‰. A clear depth gradient was observed: values in the upper 60 cm were most depleted in August (−14.1‰) and became progressively enriched, reaching their maximum (−4.7‰) by the following May. This pattern reflects direct infiltration and subsequent evaporation of monsoon rainfall. In contrast, soil water below 60-90 cm exhibited markedly dampened seasonal fluctuations, with values varying only between −11.52‰ (May) and −8.37‰ (July). This attenuation indicates a transition zone where precipitation signals are mixed and buffered. The depth profile of mean $\delta^{18}O$ further highlights this shift, showing greater variability (−10.32 ± 1.95 ‰) in the active 0-70 cm layer relative to the homogeneous deep layer below 70 cm (−9.69 ± 0.76 ‰).

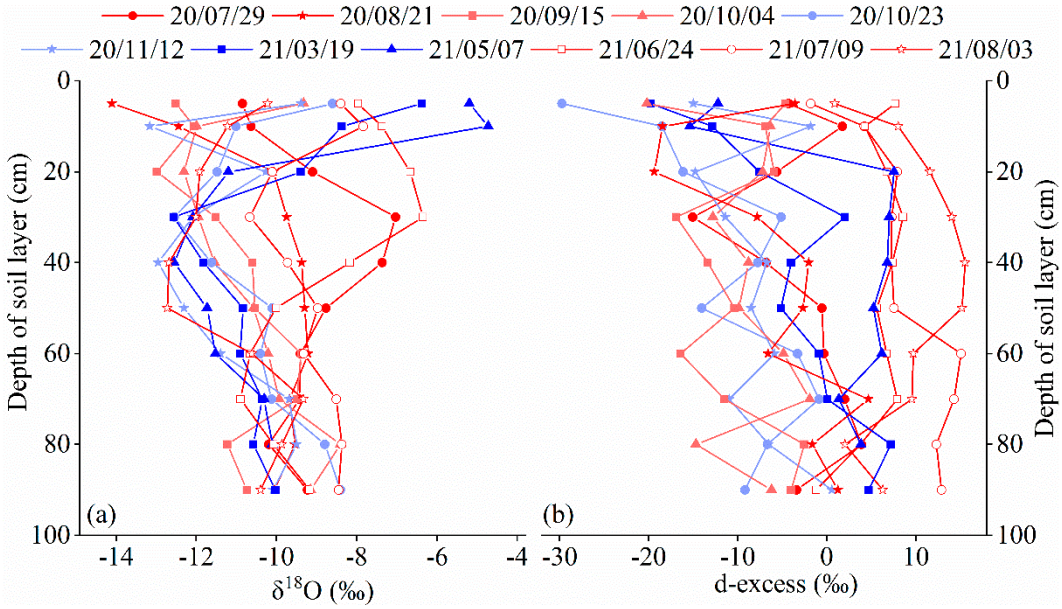

Figure 5. Variation characteristics of $\delta^{18}O$ isotopes of soil water depth profiles for eight sampling campaigns at the same location from 2020 to 2021.

© 2025 by the author(s). Distributed under a Creative Commons CC BY license.

Preprints.org (www.preprints.org) | NOT PEER-REVIEWED | Posted: 28 January 2026 doi:10.20944/preprints202601.2161.v1

The d-excess, an indicator of secondary evaporation, provided complementary insights. In the shallow zone (0-70 cm), the mean d-excess increased with depth (e.g., from −8.3 ± 9.3‰ at 5 cm to 0.2 ± 8.8‰ at 60 cm) while its variability decreased, robustly evidencing strong kinetic fractionation at the soil-atmosphere interface. Conversely, in the deep zone (70-90 cm), the mean d-excess showed a slight decreasing trend with relatively low variability (e.g., 0.8 ± 8.2‰ at 70 cm to −1.2 ± 6.0‰ at 90 cm). This dichotomy confirms that shallow soil is dominated by rapid, evaporation-influenced turnover of seasonal precipitation, whereas deep soil constitutes a stable reservoir with a longer residence time, integrating precipitation signals over extended periods. These processes create a stratified water source landscape critical for understanding plant uptake strategies.

3.5. Seasonal Variations of Plant Xylem, Stem and Leaf Water Isotopes

The seasonal variations of the $\delta^{18}O$ and d-excess as comparison with xylem and stem water during the observation period are shown in Fig. 6. There is a pronounced seasonal variation of $\delta^{18}O$ in xylem water ($\delta^{18}O_X$) and stem water ($\delta^{18}O_S$) and they are synchronized, the correlation coefficients (R) of $\delta^{18}O_X$ with $\delta^{18}O_S$ is 0.71($p < 0.001$). In the raining season, the $\delta^{18}O_X$ and $\delta^{18}O_S$ for *M. yunnanensis* rapidly decreased, while they gradually increased in the raining season, and keep a high value (Fig. 6a). The $\delta^{18}O_X$ and $\delta^{18}O_S$ was the lowest at August (Fig. 6a). Thereafter, they became more enriched as the time progressed. The $\delta^{18}O_X$ and $\delta^{18}O_S$ ranges from −11.5 ‰ to −6.92 ‰ (-9.2 ± 1.3 ‰ in average) and ranges from −10.5 ‰ to −4.5 ‰ (-7.8 ± 1.5 ‰ in average), respectively. Average monthly $\delta^{18}O$ of soil water samples were −10.1±1.71 ‰. The $\delta^{18}O_X$ is very close to soil water $\delta^{18}O$, but has a certain degree of enrichment compared to soil water. The $\delta^{18}O_X$ for *M. yunnanensis* significantly lower than stem water ($p<0.001$, $n=216$). The seasonal pattern of xylem and stem water was similar to $\delta^{2}H$ during the observations (Fig. A1). This indicates a close hydraulic linkage between xylem water and stem water within the interval. The seasonal variation of d-excess in xylem water and stem water is not significant and they are not synchronized, the correlation coefficients (R) of d-excess in xylem water with stem water is 0.1. This is because their evaporation enrichment mechanism is different (Fig. 6b).

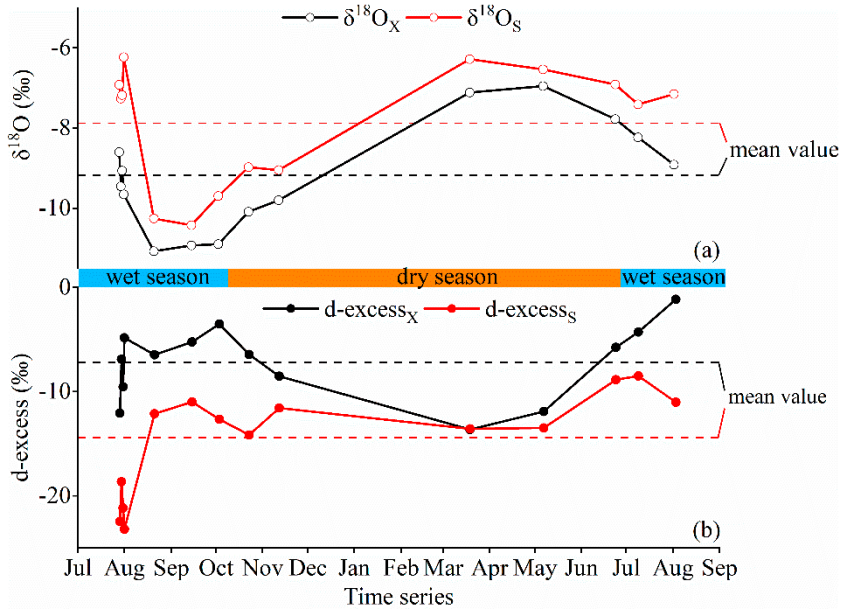

Figure 6. Seasonal variation of xylem and stem water isotopes from July 2020 to September 2021 at Kunming: (a) $\delta^{18}O$, (b) d-excess.

The seasonal variations of the $\delta^{18}O_L$ and d-excess of leaf water as comparison with leaf water enrichment during the observation period are shown in Fig. A2. Leaf water becomes enriched in heavy isotopes during transpiration due to equilibrium and kinetic effects (Flanagan et al., 1991). In general, in the rainy season (June-October), the $\delta^{18}O_L$ decreased rapidly, and after the dry season (October–June), the δ18OP increased gradually. The seasonal variations of $\delta^{18}O_L$ of leaf water are in

© 2025 by the author(s). Distributed under a Creative Commons CC BY license.

Preprints.org (www.preprints.org) | NOT PEER-REVIEWED | Posted: 28 January 2026 doi:10.20944/preprints202601.2161.v1

phase with leaf water enrichment, but d-excess of leaf water is the opposite. The seasonal pattern of leaf water enrichment was similar to δ^2H_L of leaf water during the observations (Fig. A3).

3.6. Daily and Seasonal Variations of Carbon Isotope Composition ($\delta^{13}C$) and Water Use Efficiency (WUE) in M. yunnanensis

Daily and seasonal variations dynamics of WUE reflect water requirements at different developmental stages. Here, we show daily and seasonal changes of plant $\delta^{13}C$ and WUE of *M. yunnanensis* (Fig. 7), in order to identify of its potentially driving mechanisms. The daily variation of WUE shows a "v"-shape. The low WUE value was observed from 11:00 to 17:00 (noon), the high value was observed at 9:00 and 19:00 (morning and evening), and WUE was significantly lower at 15:00 than at the other times (Fig. 7a). In a seasonal variation, the trends of WUE were rapidly increased first from July to August, from August to October (rainy season) less variable in magnitude, and then no significant decreased from October to March next (dry season), rapidly decreased from March (Fig. 7b). The seasonal variation of plant $\delta^{13}C$ is similar to WUE. The plant $\delta^{13}C$ and WUE were lowest in June under dryer atmospheric conditions of the year (Fig. 7b). Our finding that the lowest plant $\delta^{13}C$ and WUE under dryer atmospheric conditions (i.e., June), indicating that water availability is the most important limiting factors for plant growth and have been observed to affect WUE.

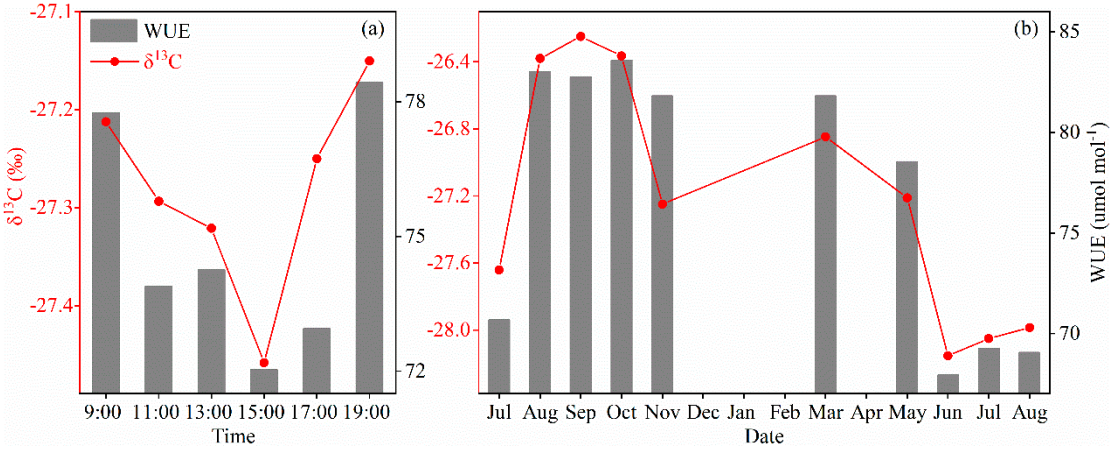

Figure 7. Daily and seasonal variation in $\delta^{13}C$ and water use efficiency (WUE) in *M. yunnanensis*.

4. Discussion

4.1. Water Source Dynamics: Creating a Stratified Resource Landscape

Soil water $\delta^{18}O$ dynamics are governed by precipitation recharge and soil evaporation, exhibiting a clear depth-dependent response to precipitation inputs (Fig. 8). Following isotopically depleted monsoon rainfall, a significant decrease in $\delta^{18}O$ in the upper 0-40 cm soil layer indicates direct infiltration and mixing, suggesting preferential flow pathways (Schwinning et al., 2004; Eggemeyer et al., 2009). During the pre-monsoon season, higher precipitation $\delta^{18}O$ and strong surface evaporation lead to enriched isotopic values in shallow soil. The depth of the evaporative front, identified per methods in Allison (1998), varied between 20-40 cm and 40-60 cm across seasons.

© 2025 by the author(s). Distributed under a Creative Commons CC BY license.

Preprints.org (www.preprints.org) | NOT PEER-REVIEWED | Posted: 28 January 2026 doi:10.20944/preprints202601.2161.v1

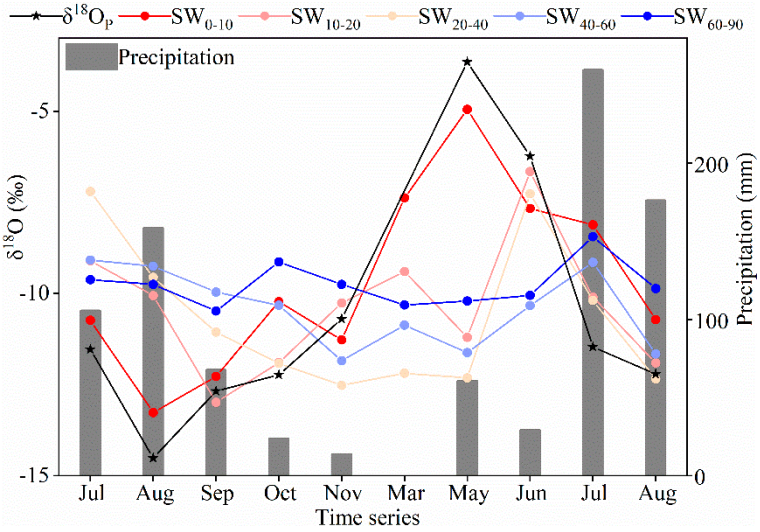

Figure 8. The monthly variation of precipitation and different depth soil water isotopes at Kunming from July 2021to August 2021.

The temporal variability of soil water $\delta^{18}O$ decreased markedly with depth. Shallow soil (0-10 cm) showed high fluctuations, tracking individual precipitation events and experiencing strong kinetic fractionation from evaporation. In contrast, soil water below 60-90 cm exhibited a significantly dampened isotopic signal, indicating the mixing of precipitation over longer timescales and dominance of liquid-phase transport (Barnes and Allison, 1983; Kendall and McDonnell, 1998). This pattern, where deeper soil acts as a buffer with a stable isotopic signature, aligns with findings in other semi-arid ecosystems (Yu et al., 2012; Dubbert et al., 2013). The stratified water source landscape created by these processes—a dynamic shallow reservoir and a stable deep reserve—forms the physical basis for plant water foraging and has direct implications for managing irrigation as an economic input, as it delineates the naturally available versus human-supplied water zones.

4.2. Water Source and Relative Contribution Proportion of M. yunnanensis

4.2.1. Qualitative Analysis of Plant Water Sources

The dual-isotope plot reveals pronounced seasonal plasticity in water uptake by *M. yunnanensis* (Fig. 9). During the wet season (July to September), xylem water $\delta^{18}O$ values closely aligned with soil water at 20-50 cm depth, indicating predominant use of shallow-to-middle soil layers. Conversely, in the dry season (October to June), xylem water isotopes matched contributions from very shallow (0-10 cm) and deeper (50-90 cm) soil sources. This adaptive strategy of shifting uptake depths in response to soil moisture availability is a well-documented drought tolerance mechanism (Rothfuss and Javaux, 2017; Zhou et al., 2015), potentially driven by root growth into deeper layers (Schwärzel et al., 2020) or reduced shallow root activity under dry conditions (Wang et al., 2021), as seen in other species (Schwendenmann et al., 2015; Kong et al., 2022). From an economic perspective, this plasticity represents a form of intrinsic resource arbitrage, allowing the tree to substitute costly irrigation with freely available soil water during drought, thereby generating direct cost savings. Occasional mismatches between xylem and soil water $\delta^{18}O$ suggest ecohydrologic separation between mobile and immobile water pools may occur even in urban settings (Brooks et al., 2010; Evaristo and McDonnell, 2017; Chen et al., 2020; Penna et al., 2022; Zhou et al., 2023), highlighting the complexity of water availability.

© 2025 by the author(s). Distributed under a Creative Commons CC BY license.

Preprints.org (www.preprints.org) | NOT PEER-REVIEWED | Posted: 28 January 2026 doi:10.20944/preprints202601.2161.v1

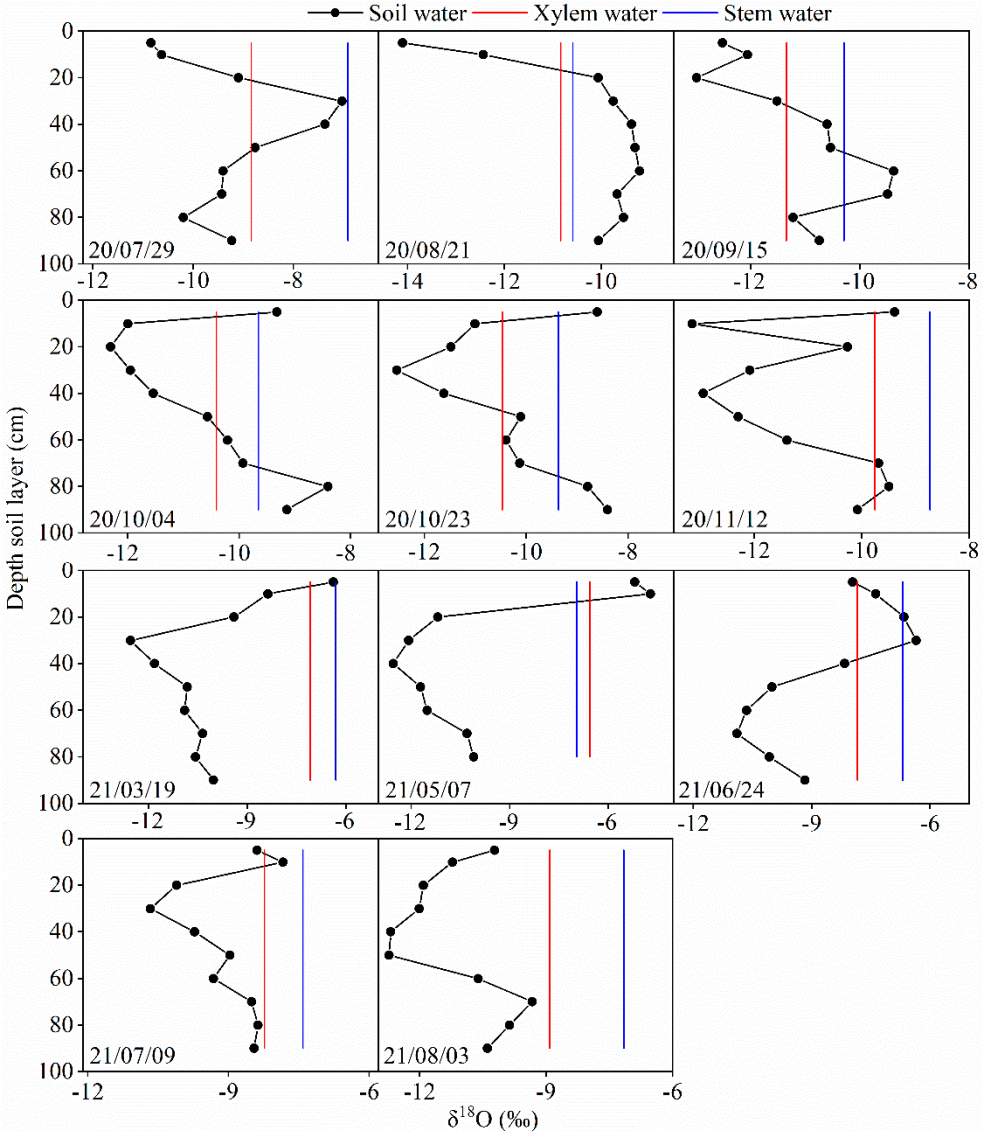

Figure 9. The relationships of $\delta^{18}O$ among soil water, xylem water and stem water from 2020-2021 at Kunming. Red line represents $\delta^{18}O$ of xylem water and blue line represents $\delta^{18}O$ of stem water.

4.2.2. Quantitative Analysis of Plant Water Sources Based on IsoSource Model

Significant isotopic differences between water pools allowed for quantitative source apportionment using a linear mixing model based on isotope mass balance (Javaux et al., 2016; Dawson et al., 1991; Rothfuss et al., 2017; Sprenger et al., 2017; Zhou et al., 2015; Schwendenmann et al., 2015). The IsoSource model output (Fig. 10) quantified that shallow soil (0-40 cm), deep soil (40-90 cm), and stem water contributed on average 30%, 40%, and 30%, respectively, over the entire period. A clear seasonal shift was quantified: deep soil water contribution increased to 40-70% in the dry season, while stem water uses also rose (mean contribution 0.35 vs. 0.23 in wet season). This shift from shallow to deep sources as soil moisture declines is a common adaptive strategy (Evaristo et al., 2019; Yang et al., 2015; Kong et al., 2022). These quantitative contributions (e.g., deep soil providing 40-70% of dry-season water) are critical for economic translation. They provide the coefficients to calculate the volume of irrigation water substituted (ΔV_irri), forming the basis for estimating operational cost savings (EV_1).

© 2025 by the author(s). Distributed under a Creative Commons CC BY license.

Preprints.org (www.preprints.org) | NOT PEER-REVIEWED | Posted: 28 January 2026 doi:10.20944/preprints202601.2161.v1

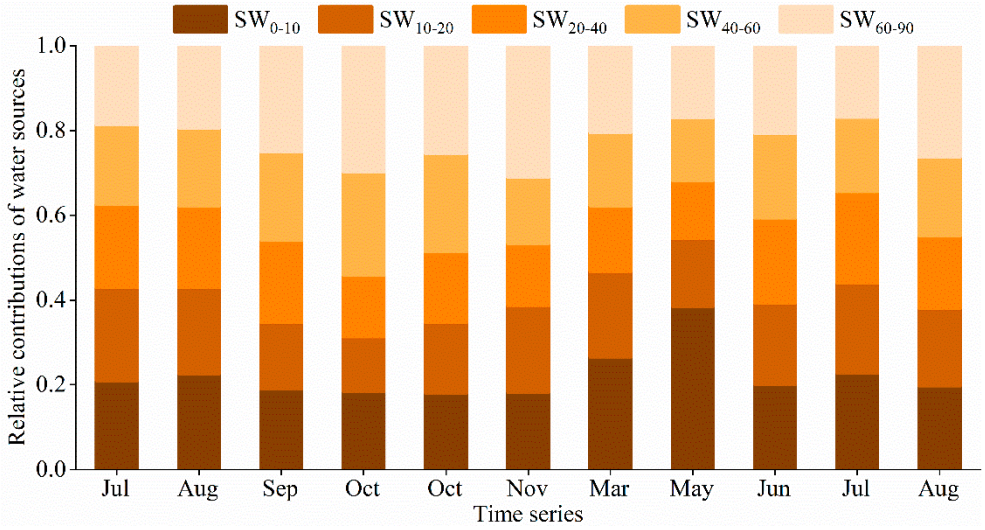

Figure 10. Relative contributions of water sources with the IsoSource model.

4.3. Water Use Strategies of M. yunnanensis: Linking Physiological Adaptations to Economic Value

The isotopic analyses delineate how *M. yunnanensis* copes with water variability. For urban resource management, the critical question is how these adaptive traits translate into measurable economic benefits. This requires reframing physiological plasticity—seasonal water source switching and dynamic WUE—within resource economics. We explicitly link the quantified ecohydrological strategies to three key economic dimensions: operational cost reduction, enhanced ecosystem service productivity, and climate resilience. This translation underscores the species' utility as "natural capital" and provides a replicable framework for cost-benefit evaluation of urban greening projects. The water foraging plasticity identified here represents a key adaptive trait that may interact with other resource acquisition strategies. For instance, recent evidence suggests a decoupling between leaf and topsoil elements in street trees, indicating complex, depth-dependent nutrient uptake (He et al., 2025). Therefore, integrating the management of water-use efficiency with nutrient dynamics within a broader "water-nutrient-carbon" framework could further optimize multiple ecosystem services simultaneously, an important direction for future urban ecological research.

4.3.1. Seasonal Water Source Plasticity for Operational Cost Mitigation

This study explicitly quantified a seasonal switching strategy (Fig.s 9, 10). During the wet season, *M. yunnanensis* primarily utilized shallow-to-middle soil water (10-50 cm), reducing reliance on supplemental irrigation. This plasticity is a well-documented strategy (Rothfuss and Javaux, 2017). In the dry season, dependence shifted to deep soil water (50-90 cm) and stem water reserves. Economically, this shift substitutes costly irrigation with naturally stored soil water (Ehleringer & Dawson, 1992), implying a substantial reduction in dry-season irrigation demand in cities like Kunming. The economic value (EV_1) is: $EV_1 = (\Delta V_irri \times P_water) + \Delta C_maint$, where ΔV_irri is irrigation water saved, P_water is the unit water price, and ΔC_maint represents saved maintenance costs (Lv et al., 2021). This positions *M. yunnanensis* as a "low-maintenance asset" that reduces long-term operational expenditures.

4.3.2. Dynamic Water-Use Efficiency Enhancing Resource Productivity

Regarding water use efficiency, $\delta^{13}C$ data revealed complex spatiotemporal dynamics (Figure 7). Diurnally, WUE showed a "V"-shaped pattern, being lower at midday (11:00-17:00) and higher in the early morning and late afternoon. This suggests that for precision irrigation scheduling, applications recommend avoid periods of lowest WUE (midday) to minimize unproductive transpirational losses and enhance the actual productivity of each unit of irrigation water (Peñuelas et al., 2011). Seasonally,

© 2025 by the author(s). Distributed under a Creative Commons CC BY license.

Preprints.org (www.preprints.org) | NOT PEER-REVIEWED | Posted: 28 January 2026 doi:10.20944/preprints202601.2161.v1

WUE increased rapidly at the beginning of the wet season (July-August) and remained relatively high throughout the dry season. The notably higher WUE in the early dry season indicates more efficient carbon assimilation per unit of water transpired under scarcity (Farquhar et al., 1989). Integrating this physiological metric into economic assessments, its value (EV_2) manifests as an increased marginal productivity of the water input. Within ecosystem service valuation frameworks, a higher WUE directly translates to greater per-tree carbon sequestration value and cooling benefits per unit of water consumed (Nowak, 2023).

In synthesis, the coordinated strategy of seasonal water source switching and enhanced WUE confers significant drought resilience, which carries intrinsic 'risk mitigation value' (EV_3), a key benefit of urban green infrastructure for climate adaptation (Escobedo et al., 2021; Baró et al., 2021). By mitigating drought-induced mortality, this strategy directly reduces tree replacement capital costs and safeguards continuous ecosystem service delivery. This value can be estimated using replacement cost methods or factored into long-term analyses as a reduced 'risk premium' (Groot et al., 2012). Therefore, selecting *M. yunnanensis* is not only an ecological decision but also a sound investment in resilient urban green infrastructure.

4.3.3. Water Use Strategies and Economic Translation

The isotopic analyses delineate how *M. yunnanensis* copes with water variability. We explicitly link these strategies to three economic dimensions.

Seasonal Water Source Plasticity for Cost Mitigation (EV_1): The quantified shift from shallow to deep soil water in the dry season substitutes costly irrigation with naturally stored water. An illustrative calculation demonstrates this logic: assuming a mature tree substitute ~1.08 m^3 of irrigation water per dry season (based on a 60% uptake shift from isotopic data and estimated transpiration) at a local water price of 6.2 CNY m^{-3}, the direct annual saving (EV_1) is approximately 6.7 CNY per tree. Scaled to a municipal planting of 10,000 trees, aggregate savings approach 67,000 CNY annually, concretizing the fiscal logic of investing in species with such plasticity.

Dynamic WUE Enhancing Resource Productivity (EV_2): The observed diurnal "V"-shaped WUE pattern and seasonal WUE enhancement indicate more efficient carbon assimilation per unit of water under scarcity. Within ecosystem service valuation frameworks, this higher WUE directly translates to greater per-tree carbon sequestration and cooling benefits per unit of water consumed (Nowak, 2023), representing an increased marginal value product of the water input (EV_2).

Coordinated Strategy for Resilience Value (EV_3): The combined strategy of source switching and enhanced WUE confers significant drought resilience. This carries intrinsic 'risk mitigation value' (EV_3) by reducing the probability and expected cost of drought-induced mortality, thereby safeguarding continuous ecosystem service delivery and avoiding replacement capital costs—a key benefit for climate adaptation planning.

4.4. Implications for Environmental and Resource Economic Theory

Beyond the specific case of *M. yunnanensis*, our integrated approach and findings offer several broader implications for environmental and resource economic theory and practice.

First, we operationalize the concept of "natural capital" at the organismal level, showing how a tree's physiological traits function as a risk-mitigating asset that generates direct financial savings (EV_1) and enhances factor productivity (EV_2). This moves valuation beyond static stock-and-flow models toward dynamic, trait-based asset pricing for urban ecosystems (Fenichel & Abbott, 2014).

Second, our framework informs the design of efficient public spending and policy instruments. By quantifying EV_3 (resilience value), it provides a rationale for "resilience premiums" in public procurement or subsidies for climate-adapted species. Furthermore, the quantified water savings (ΔV_irri) could be integrated into local water rights markets or offset schemes, creating a direct market signal for investing in water-efficient urban forests. This aligns with the theory of co-benefits internalization in environmental policy design (Shobe & Burtraw 2020).

© 2025 by the author(s). Distributed under a Creative Commons CC BY license.

Preprints.org (www.preprints.org) | NOT PEER-REVIEWED | Posted: 28 January 2026 doi:10.20944/preprints202601.2161.v1

Finally, our interdisciplinary method—using isotopic data to parameterize an economic model—exemplifies a next-generation approach to non-market valuation. It reduces reliance on stated preference methods for complex biophysical processes, instead building value estimates on observable, engineering-style measurements of resource use efficiency. This enhances the objectivity and transferability of economic assessments for green infrastructure across different institutional and climatic settings, contributing to the broader goal of integrating ecology and economics for sustainability (Polasky et al., 2019).

5. Conclusions and Policy Implications

5.1. Conclusions

This study integrated dual-water isotope (δ^2H, $\delta^{18}O$) and carbon isotope ($\delta^{13}C$) techniques to mechanistically quantify the adaptive water-use strategy of *M. yunnanensis* and, crucially, its direct economic implications—thus bridging a critical gap between ecohydrology and resource economics in urban forestry. First, isotopic evidence reveals significant seasonal plasticity in water acquisition: the species primarily utilizes shallow-to-middle soil water (10–50 cm) during the wet season but strategically shifts to deeper soil water (50–90 cm) and stem water reserves during the prolonged dry season, demonstrating a facultative foraging strategy that minimizes dependency on surface moisture. Second, analysis of $\delta^{13}C$ shows distinct diurnal and seasonal dynamics in intrinsic water-use efficiency (WUE). The characteristic diurnal "V"-shaped pattern (with lower midday WUE) and the seasonally elevated WUE during the dry period together indicate a physiological capacity for efficient carbon assimilation under water scarcity. Third, and central to our thesis, we explicitly link these physiological adaptations to a framework of tangible economic value: (1) operational cost reduction through irrigation savings enabled by source substitution; (2) enhanced resource productivity as higher WUE increases the ecosystem service output per unit of water consumed; and (3) increased resilience value by mitigating drought-induced mortality risk, thereby safeguarding public green assets. This tripartite value proposition provides a quantifiable, physiologically-grounded basis for appraising urban trees as "natural capital."

5.2. Economic Policy Recommendations

5.2.1. Develop Differentiated Precision Irrigation Schedules

Municipal greening departments should implement "seasonally differentiated irrigation" that mirrors the plastic water-use patterns of *M. yunnanensis*. This involves significantly reducing or suspending irrigation during the wet season and its immediate aftermath. Crucially, daily irrigation should be scheduled to avoid periods of lowest plant WUE (e.g., midday) to enhance application efficiency and reduce unproductive water losses (Dinar & Zilberman, 2020). This approach leverages the economic principle of optimizing input use (water) to match the temporal productivity of the biological asset (the tree), thereby maximizing the return on each unit of water invested. Implementation can be achieved by integrating the phenological and water-source phase diagrams from this study into the decision-support modules of existing urban smart irrigation systems. This integration, supported by a sensor network monitoring soil moisture and meteorological conditions, enables automated, data-driven irrigation that aligns with real-time plant physiological needs. The resulting water savings translate directly into reduced operational costs and enhanced drought resilience, providing a clear cost-benefit rationale for upfront investments in sensor and control technologies.

5.2.2. Establish a "Water Productivity"-Centric Tree Species Selection and Evaluation System

Urban planning and forestry departments should formally introduce "water use efficiency (WUE)" and "water source plasticity" as mandatory screening criteria, prioritizing native, drought-adapted species with high water-economic productivity, such as *M. yunnanensis*. For project

© 2025 by the author(s). Distributed under a Creative Commons CC BY license.

Preprints.org (www.preprints.org) | NOT PEER-REVIEWED | Posted: 28 January 2026 doi:10.20944/preprints202601.2161.v1

appraisal, the "ecosystem service value per unit of water consumption" over a species' life cycle should be calculated to inform cost-benefit analyses (Kudaya et al., 2025; McPhearson et al., 2021). The implementation pathway requires creating an open-access urban tree species eco-economic database. This database should archive key species-specific parameters (including isotopic indicators of WUE and water uptake depth, established management costs, and modeled ecosystem service values) and be coupled with user-friendly assessment tools for planners. Adopting such a physiology-informed selection system is critical. It directly addresses the widespread growth suppression in urban trees driven by water stress (Wu et al., 2025), thereby transforming green infrastructure from a water-sensitive cost center into a drought-resilient, value-generating asset.

5.2.3. Explicitly Incorporate Water-Saving Benefits into Urban Green Space Ecosystem Service Accounting

When assessing and monetizing the benefits of urban forests (e.g., carbon sequestration, cooling), the "water savings" and corresponding "water-saving value" achieved through a plant's inherent adaptive strategies must be concurrently accounted for (Song et al., 2018). This requires integrating the economic valuation framework (EV_1, EV_2) developed in this study with widely used urban forest assessment tools (e.g., i-Tree). Developing localized model modules that embed these water-saving co-benefits will make them a standard, quantifiable component of return-on-investment (ROI) analysis for green infrastructure projects, thereby strengthening the economic rationale for fiscal support and improving the accuracy of project valuations.

5.2.4. Design Incentive-Compatible Fiscal and Market Mechanisms

Governments and municipal authorities could explore establishing a "Water-Smart Green Space" certification and linked subsidy or incentive scheme. Projects that utilize certified low-water-consumption, high-resilience species (like *M. yunnanensis*) and implement precision irrigation could receive grants, tax benefits, or preferential scoring in public tenders. Furthermore, the volume of water sustainably saved by such green spaces could be quantified and potentially included in regional water rights trading or ecological compensation frameworks, transforming documented ecological performance into direct economic incentives. Implementation requires proactive collaboration between water utilities, greening departments, and finance agencies to formulate robust technical standards, verification protocols, and certification procedures.

5.2.5. Promote Cross-Sectoral Collaborative Governance and Capacity Building

The effective implementation of the above integrated policies hinges on breaking down administrative silos. We recommend establishing a permanent inter-departmental collaborative mechanism—such as an "Urban Water-Green Resource Synergy Management Group"—that includes representatives from water resource management, urban greening, public finance, and climate adaptation departments. This body should co-develop essential protocols for data sharing, joint planning guidelines, and integrated performance metrics for green infrastructure. This governance effort must be complemented by regular cross-disciplinary training and workshops to enhance mutual understanding among policymakers and practitioners of the critical links between plant physiology, hydrology, and resource economics.

Supplementary Materials: The following supporting information can be downloaded at the website of this paper posted on Preprints.org.

Authors' Contribution: Jiaojiao Han: Methodology, Writing - original draft, Writing - review & editing, Supervision, Project administration, Funding acquisition, Conceptualization. Yan Zhong: Investigation, Data curation, Software. Ziying Sun: Investigation, Methodology. Xuejie Wang: Visualization, Writing - review & editing. Yingzhu Yang: Investigation, Resources.

© 2025 by the author(s). Distributed under a Creative Commons CC BY license.

Preprints.org (www.preprints.org) | NOT PEER-REVIEWED | Posted: 28 January 2026 doi:10.20944/preprints202601.2161.v1

Acknowledgments: This study was supported by the Annual Project of the Shaanxi Provincial Social Science Foundation (Grants No. 2024D052), the Special Scientific Research Program of the Shaanxi Provincial Department of Education (Grants No. 23JK0010) and the Graduate Innovation Research Project of Baoji University of Arts and Sciences (Grants No. YJSCX25YB28).

Conflicts of Interest: The authors declare that they have no known competing financial interests or personal relationships that could have appeared to influence the work reported in this paper.

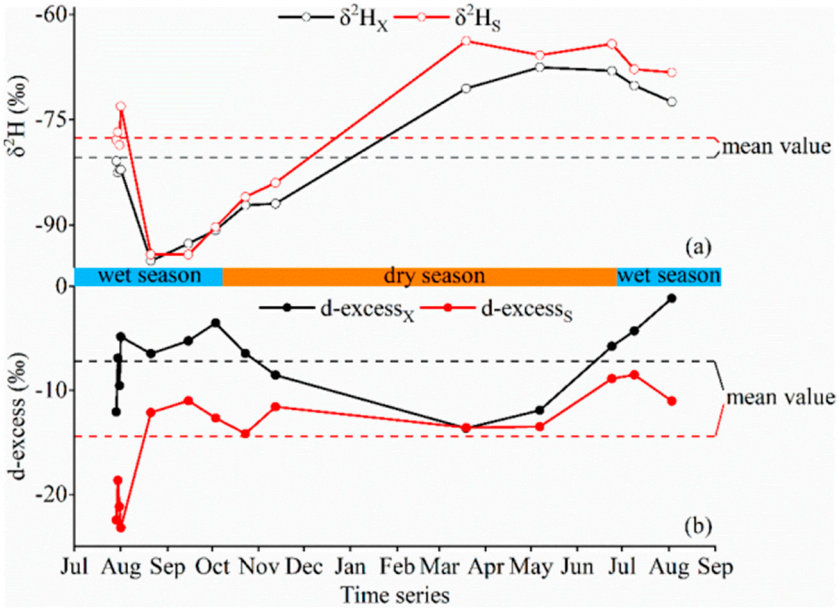

Figure A1. Seasonal variation of xylem and stem water isotopes from July 2020 to September 2021 at Kunming: (a) δ^2H, (b) d-excess.

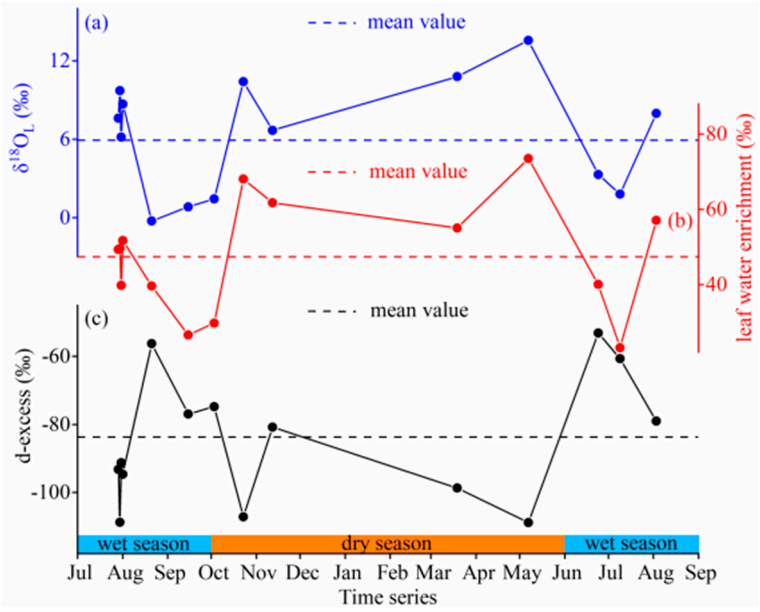

Figure A2. Seasonal variation of leaf water isotopes from July 2020 to September 2021 at Kunming: (a) $\delta^{18}O_L$, (b) leaf water enrichment, (c) d-excess.

© 2025 by the author(s). Distributed under a Creative Commons CC BY license.

Preprints.org (www.preprints.org) | NOT PEER-REVIEWED | Posted: 28 January 2026 doi:10.20944/preprints202601.2161.v1

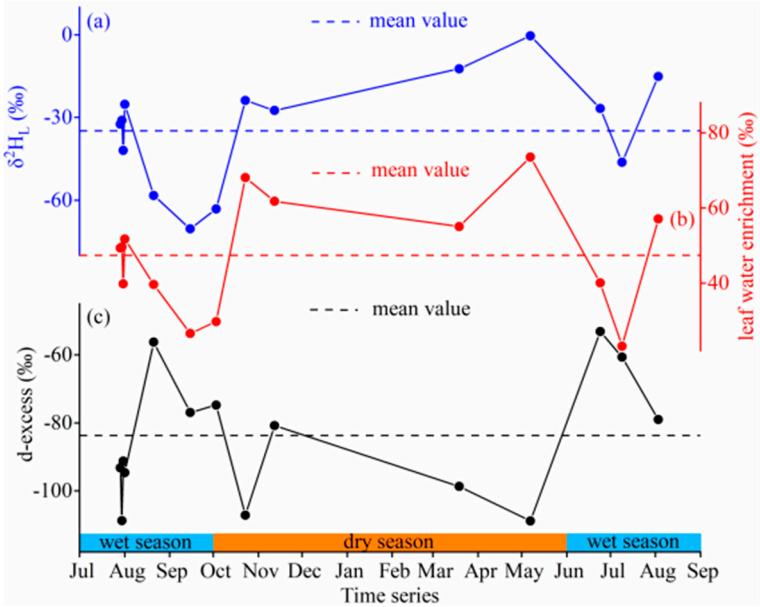

Figure A3. Seasonal variation of leaf water isotopes from 2020-2021 at Kunming: (a) δ^2H, (b) leaf water enrichment, (c) d-excess.

References

1. Allison, G.B., 1998. A review of some of the physical, chemical and isotopic techniques for estimating groundwater recharge. In: Isotope Techniques in the Study of Environmental Change. IAEA, Vienna, pp. 3–10.
2. Barnes, C.J., Allison, G.B., 1983. The distribution of deuterium and oxygen-18 in dry soils: 1. Theory. J. Hydrol. 60 (1-4), 141–156. https://doi.org/10.1016/0022-1694(83)90018-5.
3. Baró, F., Calderon-Argelich, A., Langemeyer, J., Connolly, J.J.T., 2021. Under one canopy? Assessing the distributional environmental justice implications of street tree benefits in Barcelona. Urban For. Urban Greening. 59, 126998. https://doi.org/10.1016/j.ufug.2021.126998.
4. Bi, R.X., 2018. Stable Isotope Characteristics and Water Vapor Analysis of Precipitation in Chenggong Region, Kunming. Master's Thesis. Yunnan Normal University, Yunnan, China.
5. Boyd, J., Banzhaf, S., 2007. What are ecosystem services? The need for standardized environmental accounting units. Ecol. Econ. 63 (2-3), 616–626. https://doi.org/10.1016/j.ecolecon.2007.01.002.
6. Brooks, J.R., Barnard, H.R., Coulombe, R., McDonnell, J.J., 2010. Ecohydrologic separation of water between trees and streams in a Mediterranean climate. Nat. Geosci. 3 (2), 100–104. https://doi.org/10.1038/ngeo722.
7. Chen, Y., Helliker, B.R., Tang, X., Li, F., Zhou, Y., Song, X., 2020. Stem water cryogenic extraction biases estimation in deuterium isotope composition of plant source water. Proc. Natl. Acad. Sci. U.S.A. 117 (52), 33345–33350. https://doi.org/10.1073/pnas.2014422117.
8. Craig, H., 1961. Isotopic variations in meteoric waters. Science 133 (3465), 1702–1703. https://doi.org/10.1126/science.133.3465.1702.
9. Cui, J.B., Tian, L.D., Gerlein-Safdi, C., Qu, D.M., 2017. The influence of memory, sample size effects, and filter paper material on online laser-based plant and soil water isotope measurements. Rapid Commun. Mass Spectrom. 31 (6), 509–522. https://doi.org/10.1002/rcm.7824.
10. Dawson, T.E., Ehleringer, J.R., 1991. Streamside trees that do not use stream water. Nature 350, 335–337. https://doi.org/10.1038/350335a0.
11. Dawson, T.E., Ehleringer, J.R., 1993. Isotopic enrichment of water in the "woody" tissues of plants: Implications for plant water source, water uptake, and other studies which use the stable isotopic composition of cellulose. Geochim. Cosmochim. Acta 57 (14), 3487–3492. https://doi.org/10.1016/0016-7037(93)90554-A.
12. Dinar, A., Zilberman, D. (Eds.), 2020. Handbook of Water Economics. Edward Elgar Publishing, Cheltenham, UK.

© 2025 by the author(s). Distributed under a Creative Commons CC BY license.

Preprints.org (www.preprints.org) | NOT PEER-REVIEWED | Posted: 28 January 2026 doi:10.20944/preprints202601.2161.v1

13. Dubbert, M., Cuntz, M., Piayda, A., Werner, C., 2013. Partitioning evapotranspiration – Testing the Craig and Gordon model with field measurements of oxygen isotope ratios of evaporative fluxes. J. Hydrol. 496, 142–153. https://doi.org/10.1016/j.jhydrol.2013.05.033.
14. Durodola, O.S., Rothfuss, Y., Hawes, C., Smith, J.U., Valentine, T., Geris, J., 2025. Stable water isotopes reveal modification of cereal water uptake strategies in agricultural co-cropping systems. Agric. Ecosyst. Environ. 381, 109439. https://doi.org/10.1016/j.agee.2024.109439.
15. Egerer, M., Annighöfer, P., Arzberger, S., Burger, S., Hecher, Y., Knill, V., Probst, B., Suda, M., 2024. Urban oases: the social-ecological importance of small urban green spaces. Ecosyst. People 20 (1), 2315991. https://doi.org/10.1080/26395916.2024.2315991.
16. Ehleringer, J.R., Dawson, T.E., 1992. Water uptake by plants: perspectives from stable isotope composition. Plant Cell Environ. 15 (9), 1073–1082. https://doi.org/10.1111/j.1365-3040.1992.tb01657.x.
17. Escobedo, F.J., Giannico, V., Jim, C.Y., Sanesi, G., Lafortezza, R., 2021. Urban forests, ecosystem services, green infrastructure and nature-based solutions: Nexus and evolving concepts. Urban For. Urban Greening 59, 126993. https://doi.org/10.1016/j.ufug.2021.126993.
18. Evaristo, J., Jasechko, S., McDonnell, J.J., 2019. Global separation of plant transpiration from groundwater and streamflow. Nature 525 (7567), 91–94. https://doi.org/10.1038/nature14983.
19. Evaristo, J., McDonnell, J.J., 2017. Prevalence and magnitude of groundwater use by vegetation: a global stable isotope meta-analysis. Sci. Rep. 7, 44110. https://doi.org/10.1038/srep44110.
20. Farquhar, G.D., Ehleringer, J.R., Hubick, K.T., 1989. Carbon isotope discrimination and photosynthesis. Annu. Rev. Plant Physiol. Plant Mol. Biol. 40, 503–537. https://doi.org/10.1146/annurev.pp.40.060189.002443.
21. Fenichel, E.P., Abbott, J.K., 2014. Natural capital: from metaphor to measurement. J. Assoc. Environ. Resour. Econ. 1 (1/2), 1–27. https://doi.org/10.1086/676034.
22. Flanagan, L.B., Comstock, J.P., Ehleringer, J.R., 1991. Comparison of modeled and observed environmental influences on the stable oxygen and hydrogen isotope composition of leaf water in Phaseolus vulgaris L. Plant Physiol. 96 (2), 588–596. https://doi.org/10.1104/pp.96.2.588.
23. Gao, C.X., Sun, C.J., Chen, W., Meng, S.T., Cong, J.M., 2024. Typical plant water use strategies in the eastern Loess Plateau under the background of ecological restoration. Geogr. Res. 43 (8), 1958–1976. https://doi.org/10.11821/dlyj020240149.
24. Geldern, R.V., Barth, J.A.C., 2012. Optimization of instrument setup and post-run corrections for oxygen and hydrogen stable isotope measurements of water by isotope ratio infrared spectroscopy (IRIS). Limnol. Oceanogr. Methods 10 (12), 1024–1036. https://doi.org/10.4319/lom.2012.10.1024.
25. Good, S.P., Noone, D., Bowen, G., 2015. Hydrologic connectivity constrains partitioning of global terrestrial water fluxes. Science 349 (6244), 175–177. https://doi.org/10.1126/science.aaa5931.
26. Gröning, M., Lutz, H.O., Roller-Lutz, Z., Kralik, M., Gourcy, L., Pöltenstein, L., 2012. A simple rain collector preventing water re-evaporation dedicated for δ18O and δ2H analysis of cumulative precipitation samples. J. Hydrol. 448–449, 195–200. https://doi.org/10.1016/j.jhydrol.2012.04.041.
27. Groot, R., Brander, L., van der Ploeg, S., Costanza, R., Bernard, F., Braat, L., Christie, M., Crossman, N., Ghermandi, A., Hein, L., Hussain, S., Kumar, P., McVittie, A., Portela, R., Rodriguez, L.C., ten Brink, P., van Beukering, P., 2012. Global estimates of the value of ecosystems and their services in monetary units. Ecosyst. Serv. 1 (1), 50–61. https://doi.org/10.1016/j.ecoser.2012.07.005.
28. Han, J.J., Tian, L.D., Cai, Z.Y., Ren, W., Liu, W.W., Li, J., Tai, J.R., 2022. Season-specific evapotranspiration partitioning using dual water isotopes in a *Pinus yunnanensis* ecosystem, southwest China. J. Hydrol. 608, 127852. https://doi.org/10.1016/j.jhydrol.2021.127852.
29. He, T., Du, E., Yang, X., Guo, Y., Xia, N., de Vries, W., 2025. Urban-rural shifts in elemental composition in leaves and topsoil of street trees in a subtropical city of China. Urban For. Urban Greening. 104, 128677.
30. Javaux, M., Rothfuss, Y., Vanderborght, J., Vereecken, H., Brüggemann, N., 2016. Isotopic composition of plant water sources. Nature 536, E1–E3. https://doi.org/10.1038/nature18946.
31. Kendall, C., McDonnell, J.J. (Eds.), 1998. Isotope Tracers in Catchment Hydrology. Elsevier, Amsterdam.
32. Kong, Y., Wang, L., Wang, S., Zhao, X., 2022. Seasonal variations in water uptake and transpiration of plants: Evidence from stable isotopes and modeling. Agric. For. Meteorol. 315, 108818. https://doi.org/10.1016/j.agrformet.2022.108818.

© 2025 by the author(s). Distributed under a Creative Commons CC BY license.

Preprints.org (www.preprints.org) | NOT PEER-REVIEWED | Posted: 28 January 2026 doi:10.20944/preprints202601.2161.v1

33. Kudaya, F.S., König, A., Fuchs-Hanusch, D., 2025. Analyzing variability and possible trends in NDVI for urban water management: A remote-sensing approach for long term monitoring of green infrastructure. EGU General Assembly 2025, Vienna, Austria.
34. Lai, Y., Kang, J.Q., Xie, H.N., 2022. Runoff collection and irrigation utilization cost of park green space in semi humid area: a case study of the green space of East Binhu Road in Qian'an City. J. Beijing For. Univ. 44 (5), 115–123.
35. Li, B., Shi, P., Li, Z., 2024. Partitioning and controlling factors of evapotranspiration: 1. Hydrological modeling constrained with isotope-based water balance decoupling. Agric. Ecosyst. Environ. 364, 108908. https://doi.org/10.1016/j.agee.2024.108908.
36. Liu, J., Penna, D., Xiao, X., Guo, L., Chen, G., Jiang, C., Wu, H., Wang, S., Jiang, Z., Jin, Z., 2025. Towards an isotope-based conceptual catchment model of the ecohydrological cycle in the Critical Zone on the Loess Plateau of China. J. Hydrol. 656, 133042. https://doi.org/10.1016/j.jhydrol.2025.133042.
37. Liu, X.M., Zhang, D., 2012. Trend analysis of reference evapotranspiration in northwest China: the roles of changing wind speed and surface air temperature. Hydrol. Process. 27 (26), 3941–3948. https://doi.org/10.1002/hyp.9527.
38. Lv, C., He, Y., Zhang, W., Gu, C., Li, Y., Yan, D., 2021. Quantitative Analysis of Eco-economic Benefits of Urban Reclaimed Water Greening Based on Emergy Theory. Water Resour. Manag. 35 (14), 5029–5047. https://doi.org/10.1007/s11269-021-02983-4.
39. Martínez-Sancho, E., Dorado-Liñán, I., Gutiérrez Merino, E., Matiu, M., Helle, G., Heinrich, I., Menzel, A., 2017. Increased water-use efficiency translates into contrasting growth patterns of Scots pine and sessile oak at their southern distribution limits. Glob. Change Biol. 24 (3), 1012–1028. https://doi.org/10.1111/gcb.13937.
40. Matias, P., Manuela, M.D.S., Teigo, J., Duarte, A., 2025. Urban vegetation benefits in mediterranean cities for climate change adaptation and water usage efficiency – a case study in Algarve, Portugal. Front. Environ. Sci. 13, 1520934. https://doi.org/10.3389/fenvs.2025.1520934.
41. Maxwell, T.M., Silva, L.C.R., Horwath, W.R., 2018. Integrating effects of species composition and soil properties to predict shifts in montane forest carbon-water relations. Proc. Natl. Acad. Sci. U.S.A. 115 (18), E4219–E4226. https://doi.org/10.1073/pnas.1718864115.
42. Nowak, D.J., 2023. Understanding i-Tree: Summary of programs and methods. Gen. Tech. Rep. NRS-200. U.S. Department of Agriculture, Forest Service, Northern Research Station, Madison, WI. https://doi.org/10.2737/NRS-GTR-200.
43. Penna, D., Hopp, L., Scandellari, F., Allen, S.T., Benettin, P., Beyer, M., Geris, J., Klaus, J., Marshall, J.D., Schwendenmann, L., Volkmann, T.H.M., Freyberg, J., Amin, A., Ceperley, N., Engel, M., Frentress, J., Giambastiani, Y., McDonnell, J.J., Zuecco, G., Llorens, P., Siegwolf, R.T.W., Dawson, T.E., Kirchner, J.W., 2022. Ideas and perspectives: Tracing terrestrial ecosystem water fluxes using hydrogen and oxygen stable isotopes – challenges and opportunities from an interdisciplinary perspective. Biogeosciences 19 (19), 4839–4869. https://doi.org/10.5194/bg-19-4839-2022.
44. Peñuelas, J., Canadell, J.G., Ogaya, R., 2011. Increased water-use efficiency during the 20th century did not translate into enhanced tree growth. Glob. Ecol. Biogeogr. 20 (4), 597–608. https://doi.org/10.1111/j.1466-8238.2010.00608.x.
45. Polasky, S., Kling, C.L., Levin, S.A., Carpenter, S.R., Daily, G.C., Ehrlich, P.R., ... Lubchenco, J., 2019. Role of economics in analyzing the environment and sustainable development. Proc. Natl. Acad. Sci. U.S.A. 116 (12), 5233–5238. https://doi.org/10.1073/pnas.1901616116.
46. Qi, P., Sun, J., Zhang, G., 2025. Optimal allocation of water and land resources considering crop water demand process from the perspective of water-carbon-economy nexus. J. Hydrol. 654, 132831. https://doi.org/10.1016/j.jhydrol.2025.132831.
47. Quade, M., Klosterhalfen, A., Graf, A., Brüggemann, N., Hermes, N., Vereecken, H., Rothfuss, Y., 2019. In-situ monitoring of soil water isotopic composition for partitioning of evapotranspiration during one growing season of sugar beet (Beta vulgaris). Agric. For. Meteorol. 266-267, 53–64. https://doi.org/10.1016/j.agrformet.2018.12.002.

© 2025 by the author(s). Distributed under a Creative Commons CC BY license.

Preprints.org (www.preprints.org) | NOT PEER-REVIEWED | Posted: 28 January 2026 doi:10.20944/preprints202601.2161.v1

48. Rothfuss, Y., Javaux, M., 2017. Reviews and syntheses: Isotopic approaches to quantify root water uptake: a review and comparison of methods. Biogeosciences 14 (8), 2199–2224. https://doi.org/10.5194/bg-14-2199-2017.
49. Rozanski, K., Araguás-Araguás, L., Gonfiantini, R., 1993. Isotopic patterns in modern global precipitation. In: Climate Change in Continental Isotopic Records. Geophys. Monogr. Ser., vol. 78. American Geophysical Union, Washington, D.C., pp. 1–36.
50. Salmani, H., Gil-García, L., González-López, H., 2025. Integrating hydrological and economic modeling to assess the impacts of adaptation policies. EGUsphere [preprint]. https://doi.org/10.5194/egusphere-egu24-8661.
51. Santos, M.S.N.D., Wancura, J.H.C., Oro, C.E.D., Vezaro, F.D., Ody, L.P., Tres, M.V., Zabot, G.L., 2025. Urban agriculture and water recycling: A comprehensive outlook on current panorama. Environ. Dev. 54, 101156. https://doi.org/10.1016/j.envdev.2025.101156.
52. Schwärzel, K., Zhang, L., Streudle, G., Bernhofer, C., 2020. The distributed process-based watershed model BROOK90 for simulating water, energy, and matter fluxes: A review. Water 12 (12), 3406. https://doi.org/10.3390/w12123406.
53. Schwendenmann, L., Pendall, E., Sanchez-Bragado, R., Kunert, N., Hölscher, D., 2015. Tree water uptake in a tropical plantation varying in tree diversity: Interspecific differences, seasonal shifts and complementarity. Ecohydrology 8 (1), 1–12. https://doi.org/10.1002/eco.1479.
54. Schwinning, S., Sala, O.E., 2004. Hierarchy of responses to resource pulses in arid and semi-arid ecosystems. Oecologia 141 (2), 211–220. https://doi.org/10.1007/s00442-004-1520-8.
55. Shi, W., Cheng, K.M., Wang, J.S., 2021. Progress on the accounting purpose-based ecosystem service valuation methods. Chin. J. Appl. Ecol. 32 (4), 1518–1530. https://doi.org/10.13287/j.1001-9332.202104.011.
56. Shobe, W.M., Burtraw, D., 2020. Rethinking environmental federalism in a warming world. Environ. Resour. Econ. 77 (4), 679 – 710. https://doi.org/10.1007/s10640-020-00514-0.
57. Song, P.X., Tan, Y.P., Edwards, P., Richards, D., 2018. The economic benefits and costs of trees in urban forest stewardship: A systematic review. Urban For. Urban Greening 29, 162–170. https://doi.org/10.1016/j.ufug.2017.11.017.
58. Sprenger, M., Leistert, H., Gimbel, K., Weiler, M., 2016. Illuminating hydrological processes at the soil-vegetation-atmosphere interface with water stable isotopes. Rev. Geophys. 54 (3), 674–704. https://doi.org/10.1002/2015RG000515.
59. Sprenger, M., Tetzlaff, D., Soulsby, C., 2017. Soil water stable isotopes reveal evaporation dynamics at the soil-plant-atmosphere interface of the critical zone. Hydrol. Earth Syst. Sci. 21 (7), 3839–3858. https://doi.org/10.5194/hess-21-3839-2017.
60. United Nations Environment Programme, 2021. Making Peace with Nature: A scientific blueprint to tackle the climate, biodiversity and pollution emergencies. UNEP, Nairobi. https://www.unep.org/resources/making-peace-nature.
61. Wang, J., Fu, B., Lu, N., Zhang, L., 2021. Seasonal variation in water uptake patterns of three alpine species based on stable isotopes in the semi-arid Heihe River Basin. J. Hydrol. 598, 126248. https://doi.org/10.1016/j.jhydrol.2021.126248.
62. Wang, S.J., Wang, H., Li, J.H., 2016. Effects of soil temperature and moisture on the temporal variations of soil respiration under forest and lawn in Kunming. J. Northwest For. Univ. 31 (5), 306–310.
63. Wilson, K.B., Hanson, P.J., Mulholland, P.J., Baldocchi, D.D., Wullschleger, S.D., 2001. A comparison of methods for determining forest evapotranspiration and its components: sap-flow, soil water budget, eddy covariance and catchment water balance. Agric. For. Meteorol. 106 (2), 153–168. https://doi.org/10.1016/S0168-1923(00)00199-4.
64. Wu, Q., Zaw, Z., Yang, J., Yang, R., Li, Z., Hauer, R.J., Li, H., Fan, Z., Lu, H., Sterck, F., 2025. Urbanization associated with greater tree growth declines in urban than in rural forests. Urban For. Urban Greening. 104, 128599.
65. Xu, X.J., Zhou, G.M., Liu, S.G., Du, H.Q., Mo, L.F., Shi, Y.J., Jiang, H., Zhou, Y.F., Liu, E.B., 2013. Implications of ice storm damages on the water and carbon cycle of bamboo forests in southeastern China. Agric. For. Meteorol. 177, 35–45. https://doi.org/10.1016/j.agrformet.2013.04.005.

© 2025 by the author(s). Distributed under a Creative Commons CC BY license.

Preprints.org (www.preprints.org) | NOT PEER-REVIEWED | Posted: 28 January 2026 doi:10.20944/preprints202601.2161.v1

66. Yan, W., Zhong, Y., Zheng, S., Shangguan, Z., 2016. Linking plant leaf nutrients/stoichiometry to water use efficiency on the Loess Plateau in China. Ecol. Eng. 87, 124–131. https://doi.org/10.1016/j.ecoleng.2015.11.034.
67. Yang, B., Wen, X., Sun, X., 2015. Seasonal variations in depth of water uptake for a subtropical coniferous plantation subjected to drought in an East Asian monsoon region. Agric. For. Meteorol. 201, 218–228. https://doi.org/10.1016/j.agrformet.2014.11.020.
68. Yang, X., Duan, C., Chen, B., Wang, H., 2025. The socio-economic value of urban green spaces in mitigating waterlogging and enhancing well-being. Resour. Conserv. Recycl. 212, 108010. https://doi.org/10.1016/j.resconrec.2024.108010.
69. Yu, T., Feng, Q., Si, J., Zhang, X., Zhao, C., 2012. Using stable isotopes to analyze the water use strategies of Tamarix ramosissima in the Heihe River Basin, China. Arid Land Res. Manag. 26 (4), 330–343. https://doi.org/10.1080/15324982.2012.709220.
70. Zhang, B.J., Li, Z.X., Feng, Q., Zhang, B.T., Gui, J., 2022. A review of isotope ecohydrology in the cold regions of Western China. Sci. Total Environ. 857 (Pt 2), 159438. https://doi.org/10.1016/j.scitotenv.2022.159438.
71. Zhou, H., Zhao, W., Zhang, G., 2015. Varying water utilization of Haloxylon ammodendron plantations in a desert-oasis ecotone. Hydrol. Process. 31 (4), 825–835. https://doi.org/10.1002/hyp.11060.
72. Zhou, Y., Wang, L., Liu, X., Zhang, Y., Chen, H., 2023. Contrasting water use strategies of two desert shrubs along a precipitation gradient: Evidence from stable isotopes. J. Hydrol. 617 (Part B), 129075. https://doi.org/10.1016/j.jhydrol.2022.129075.
73. Zhu, Y.M., Zhao, D., Yang, R.W., 2021. Interannual coverability of summer monsoon precipitation in Yunnan, China, and diabatic heating anomalies over the Arabian Sea–Bay of Bengal. Clim. Dyn. 57 (7-8), 2063–2077. https://doi.org/10.1007/s00382-021-05794-w.

Disclaimer/Publisher's Note: The statements, opinions and data contained in all publications are solely those of the individual author(s) and contributor(s) and not of MDPI and/or the editor(s). MDPI and/or the editor(s) disclaim responsibility for any injury to people or property resulting from any ideas, methods, instructions or products referred to in the content.

© 2025 by the author(s). Distributed under a Creative Commons CC BY license.